ACS central science

Research Article

Cite This: ACS Cent. Sci. 2018, 4, 362−371

Shuttling Rates, Electronic States, and Hysteresis in a Ring-in-Ring Rotaxane

Mark C. Lipke,[†] Yilei Wu,[‡] Indranil Roy,[‡] Yuping Wang,[‡] Michael R. Wasielewski,[‡] and J. Fraser Stoddart*[,‡]

[†]Department of Chemistry and Chemical Biology, Rutgers, The State University of New Jersey, 610 Taylor Road, Piscataway, New Jersey 08854, United States

[‡]Department of Chemistry, Northwestern University, 2145 Sheridan Road, Evanston, Illinois 60208, United States

Supporting Information

ABSTRACT: The trisradical recognition motif between a 4,4′-bipyridinium radical cation and a cyclo-bis-4,4′-bipyridinium diradical dication has been employed previously in rotaxanes to control their nanomechanical and electronic properties. Herein, we describe the synthesis and characterization of a redox-active ring-in-ring [2]rotaxane **BBR**·8PF$_6$ that employs a tetraradical variant of this recognition motif. A square-shaped bis-4,4′-bipyridinium cyclophane is mechanically interlocked around the dumbbell component of this rotaxane, and the dumbbell itself incorporates a smaller bis-4,4′-bipyridinium cyclophane into its covalently bonded structure. This small cyclophane serves as a significant impediment to the shuttling of the larger ring across the dumbbell component of **BBR**$^{8+}$, whereas reduction to the tetraradical tetracationic state **BBR**$^{4(+\bullet)}$ results in strong association of the two cyclophanes driven by two radical-pairing interactions. In these respects, **BBR**·8PF$_6$ exhibits qualitatively similar behavior to its predecessors that interconvert between hexacationic and trisradical tricationic states. The rigid preorganization of two bipyridinium groups within the dumbbell of **BBR**·8PF$_6$ confers, however, two distinct properties upon this rotaxane: (1) the rate of shuttling is reduced significantly relative to those of its predecessors, resulting in marked electrochemical hysteresis observed by cyclic voltammetry for switching between the **BBR**$^{8+}$/**BBR**$^{4(+\bullet)}$ states, and (2) the formally tetraradical form of the rotaxane, **BBR**$^{4(+\bullet)}$, exhibits a diamagnetic ground state, which, as a result of the slow shuttling motions within **BBR**$^{4(+\bullet)}$, has a long enough lifetime to be characterized by ^{1}H NMR spectroscopy.

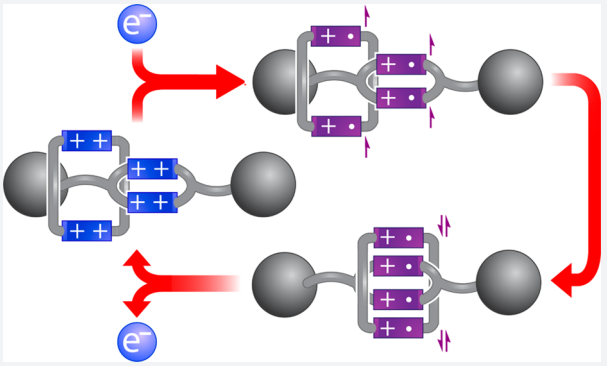

INTRODUCTION

Mechanically interlocked molecules[1−17] (MIMs) are of interest on account of their unique chemical,[18−22] physical,[23−27] and electronic properties.[28−36] Their distinct characteristics have been employed in a variety of advanced nanomaterials, including nanoswitches,[28−32,36−42] molecular muscles,[43−48] molecular motors,[49−51] and nanoscopic stabilized radicals.[33,34,52,53] The features of these nanomaterials are realized, at least in part, by the control over the individual component's relative motion,[6] or lack thereof, that is a consequence of the mechanical link. Thus, it is of interest to develop even more precise methods for controlling the movement and spatial arrangement of the mechanically interlocked components, while paradoxically, the practical demands of possible applications[54] require that this control be achieved using minimal synthetic effort.

The use[55−57] of radical-pairing interactions[58−62] to template the formation of catenanes and rotaxanes has been a significant recent development[55−57] in the field of functional MIMs, not only offering a facile means to their synthesis but also imbuing the products with distinct electronic properties[33,34] and stimulus responsive motion.[32,33,48] This research began with the discovery[63,64] that the dicationic diradical state of cyclobis(paraquat-*p*-phenylene), **CBPQT**$^{2(+\bullet)}$, and the monocationic monoradical state of methyl viologen, **MV**$^{+\bullet}$, form a strongly associated tricationic trisradical complex [**CBPQT**⊂**MV**]$^{3(+\bullet)}$. Variations of this host−guest complex have been used (Scheme 1) to template[55−57] the formation of a variety of MIMs, such as the [2]rotaxane[57] **CBPQT-RV-**[2]**R**$^{6+}$ and the homo[2]catenane[34] ***bis*-CBPQT-**[2]**C**$^{(7+)(1\bullet)}$. The restricted motion of the interlocked cyclophanes in ***bis*-CBPQT-**[2]**C**$^{(7+)(1\bullet)}$ results in this MIM exhibiting an air-stable radical state,[34] while reduction and oxidation of **CBPQT-RV-**[2]**R**$^{6+}$ toggle between strong attraction and repulsion of its viologen components.[57] These features are promising for applications in molecular electronics[32,36]/muscles[47,48]/machines,[65,66] but there are currently limitations. For example, ***bis*-CBPQT-**[2]**C**$^{(7+)(1\bullet)}$ exhibits only one translational state,[34] while **CBPQT-RV-**[2]**R**$^{6+}$ exhibits[33] very rapid redox-stimulated shuttling behavior. As a consequence, both MIMs have limited potential for hysteretic[28,30,32] electrochemical behavior

Received: November 6, 2017
Published: March 2, 2018

DOI: 10.1021/acscentsci.7b00535
ACS Cent. Sci. 2018, 4, 362−371

Scheme 1. Structural Formulas and Space-Filling Representations of Examples of Radical Host–Guest Complexes and Their Mechanically Interlocked Derivatives

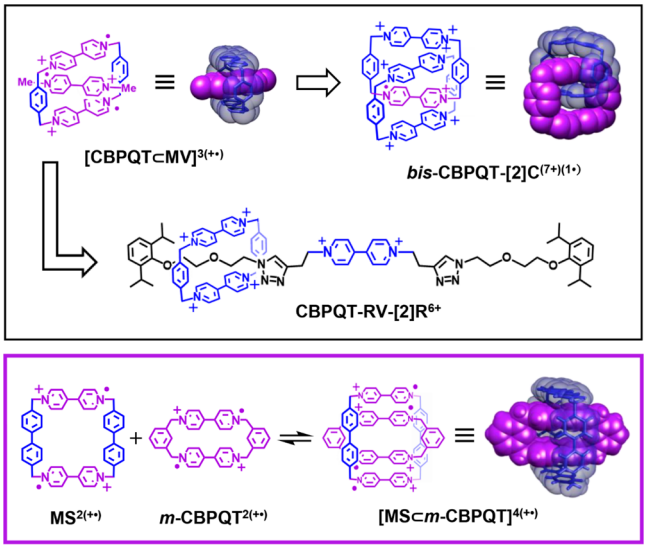

that is desired for electronic applications. Additionally, rotaxanes based on the trisradical complex $[\mathbf{CBPQT}\subset\mathbf{MV}]^{3(+\bullet)}$ are inherently paramagnetic in their reduced states, a property which prevents characterization of these states by the easily accessible and well-developed techniques of NMR spectroscopy.[67]

The radical ring-in-ring complex[68] $[\mathbf{MS}\subset m\text{-}\mathbf{CBPQT}]^{4(+\bullet)}$—formed between a small dicationic diradical cyclophane[59] ***m*-CBPQT**$^{2(+\bullet)}$ and a dicationic diradical molecular square[69] $\mathbf{MS}^{2(+\bullet)}$—offers a possible solution to the shortcomings of the first generation of radical MIMs. Although $[\mathbf{MS}\subset m\text{-}\mathbf{CBPQT}]^{4(+\bullet)}$ resembles (Scheme 1) an expanded version of $[\mathbf{CBPQT}\subset\mathbf{MV}]^{3(+\bullet)}$, the former was found[68] to exhibit much slower rates of association/dissociation. This second generation complex is also comparable to ***bis*-CBPQT-[2]C**$^{(7+)(1\bullet)}$ insofar as both are composed of two *bis*-viologen cyclophanes, but unlike the catenane, MIMs based on $[\mathbf{MS}\subset m\text{-}\mathbf{CBPQT}]^{4(+\bullet)}$ have the potential to display bistability. Lastly, $[\mathbf{MS}\subset m\text{-}\mathbf{CBPQT}]^{4(+\bullet)}$ is a ground-state singlet, suggesting that NMR spectroscopy might be used to characterize MIMs designed around this complex. Herein, we describe a ring-in-ring rotaxane—a simple but as yet uncommon[16,70,71] type of MIM—which incorporates a derivative of ***m*-CBPQT**$^{2(+\bullet)}$ in its dumbbell component as a recognition unit for $\mathbf{MS}^{2(+\bullet)}$.

RESULTS AND DISCUSSION

Synthesis of a Ring-In-Ring Rotaxane BBR·8PF$_6$. In order to synthesize a rotaxane utilizing the host–guest complex $[\mathbf{MS}\subset m\text{-}\mathbf{CBPQT}]^{4(+\bullet)}$ as a template, it was, first of all, necessary to prepare a derivative of the ***m*-CBPQT**$^{2(+\bullet)}$ guest that would be amenable to further functionalization. Since copper-catalyzed alkyne–azide cycloaddition (CuAAC) has recently been shown[57] to be useful for synthesizing radically templated MIMs, a bis-azide substituted cyclophane ***m*-N$_3$-CBPQT**·4PF$_6$ was targeted.

The synthesis (Scheme 2) of ***m*-N$_3$-CBPQT**·4PF$_6$ was accomplished in four steps, starting from the known[72] 3,5-bis(hydroxymethyl)aniline (**1**). This starting material can be obtained commercially, or by employing a published

Scheme 2. Synthesis of *m*-N$_3$-CBPQT·4PF$_6$

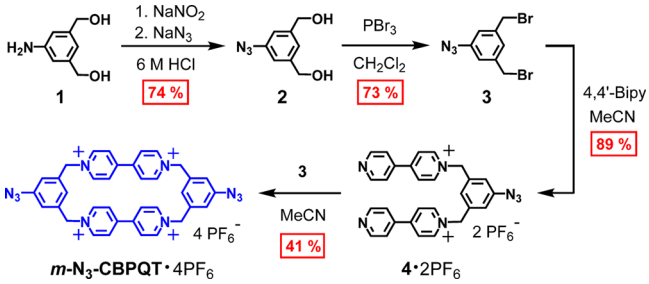

procedure[72] involving the reduction of inexpensive dimethyl 5-aminoisophthalate. The intermediate compounds **2**, **3**, and **4**, were obtained in good yields and, moreover, could be purified by crystallization or by washing with an appropriate solvent. The target cyclophane, ***m*-N$_3$-CBPQT**·4PF$_6$, was also obtained pure without the need for chromatography. A mixed Br^-/PF_6^- salt of the product precipitated from the reaction mixture in nearly pure form; additional crops were obtained by concentrating the supernatant. Pure ***m*-N$_3$-CBPQT**·4PF$_6$ was obtained in 41% yield after washing the precipitate sparingly with MeCN, followed by salt metathesis with aqueous NH_4PF_6. This relatively easy synthesis is notable since, at the outset, it seemed possible that incorporating a cyclophane component into the dumbbell of a rotaxane would introduce a considerable synthetic burden at an early stage.

Scheme 3 depicts the use of ***m*-N$_3$-CBPQT**·4PF$_6$ in the synthesis of the Box-in-Box-Rotaxane·8PF$_6$ (**BBR**·8PF$_6$), a

Scheme 3. Synthesis of the Box-In-Box Rotaxane BBR·8PF$_6$

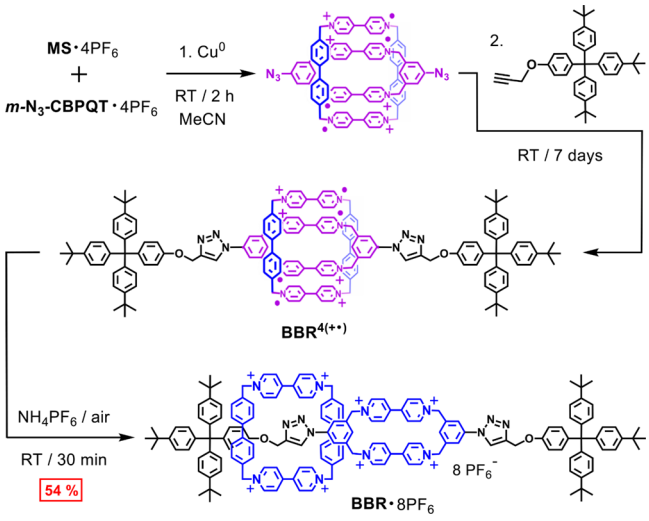

name that recognizes the common use[73] of the term "box" to refer to rigid viologen-based cyclophanes. Copper powder was used as a reducing agent in order to generate the host–guest complex $[\mathbf{MS}\subset m\text{-}\mathbf{N_3\text{-}CBPQT}]^{4(+\bullet)}$ from a 1:1 ratio mixture of ***m*-N$_3$-CBPQT**·4PF$_6$ and **MS**·4PF$_6$ in MeCN. As reported previously in the synthesis[57] of **CBPQT-RV-[2]R**·6PF$_6$, this reduction generates $(MeCN)_4Cu^+$ as a byproduct, which mediates the cycloadditions between $[\mathbf{MS}\subset m\text{-}\mathbf{N_3\text{-}CBPQT}]^{4(+\bullet)}$ and a bulky alkyne. The tetracationic tetraradical rotaxane $\mathbf{BBR}^{4(+\bullet)}$, which is formed initially, is converted into its octacationic state, $\mathbf{BBR}^{8+}$, upon oxidation with air. Examination of the crude product by ^{1}H NMR spectroscopy

DOI: 10.1021/acscentsci.7b00535
ACS Cent. Sci. 2018, 4, 362–371

indicated that 70−80% of ***m*-N$_3$-CBPQT**·4PF$_6$ was converted to the rotaxane, while the remainder was converted to the *m*-Box-Dumbbell^{4+} (***m*-BDB**$^{4+}$) component that was not encircled by the molecular square. The rotaxane was isolated in 54% yield after a series of solvent washes, salt metathesis steps, crystallization of the tetracationic tetraradical form, and reoxidation with air. The purification of **BBR**·8PF$_6$ is, thus, more complicated than that for ***m*-N$_3$-CBPQT**·4PF$_6$, but the individual steps are operationally simple and the need for chromatography is once again avoided.

Spectroscopic Characterization of BBR^{8+} and BBR$^{4(+\bullet)}$. The mechanically interlocked nature of the rotaxane was confirmed by ESI-HRMS, DOSY NMR spectroscopy, and UV−vis−NIR dilution measurements of its reduced **BBR**$^{4(+\bullet)}$ state. See the synthetic details and Figures S3 and S10. The ^{1}H NMR spectrum (Figure 1) also reveals the mechanically

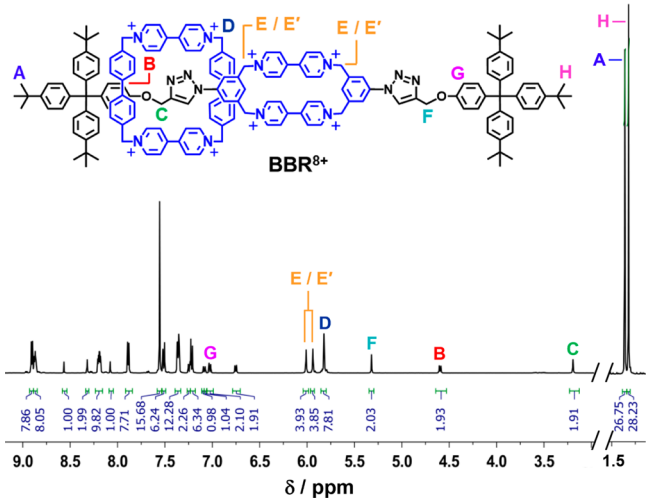

Figure 1. ^{1}H NMR spectrum of a CD$_3$CN solution of **BBR**·8PF$_6$. The spectrum is abridged in the region of the residual CD$_2$HCN and HOD resonances, while all of the signals for the **BBR**$^{8+}$ cation are displayed. Selected resonances are labeled in order to illustrate the coconstitutional asymmetry of the rotaxane. See Figure S1 for full ^{1}H NMR spectroscopic assignments.

interlocked nature of **BBR**$^{8+}$. All the resonances of the dumbbell component of **BBR**$^{8+}$ exhibit anisochronicity because the molecular square is confined, at least on the NMR exchange time scale, to one end of the dumbbell. The asymmetry is observed most clearly in (i) the −CH$_2$O− proton resonances and (ii) the ortho Ar−H signals of the phenolic group. These signals are shifted upfield considerably for the side of the dumbbell that is encircled by the molecular square, indicating that this electron deficient cyclophane resides over the electron rich ether unit.

The proton resonances of **BBR**$^{8+}$ exhibit only slight broadening of ≤2 Hz at half-height in ^{1}H NMR spectra that were collected at 75 °C compared with those recorded at 25 °C in CD$_3$CN. See Figures S11 and S12. Significant broadening, let alone coalescence, was not observed at 75 °C, even for the pair of potentially exchangeable resonances that exhibited the smallest separation (ca. 6.5 Hz at 500 MHz) from each other. From this latter observation, it can be inferred[74] that the molecular square translates across the cyclophane portion of the dumbbell at a rate, k_{ex}, that is $\ll 29$ s^{-1} at 75 °C. Furthermore, it can be inferred that the degenerate coconformations of **BBR**$^{8+}$ have lifetimes of >1 s at 25 °C. In contrast, the ^{1}H NMR spectrum of **CBPQT-RV-R**·6PF$_6$ in CD$_3$CN exhibits significant broadening/coalescence for several of the signals at 25 °C. Although the rates[33,57] of shuttling of rings along dumbbells in hexacationic rotaxanes of this type are slower in CD$_3$COCD$_3$ solutions, fast shuttling is observed[33,57] for these rotaxanes, even in this solvent, at elevated temperatures. The differences in the shuttling rates observed for hexacationic rotaxanes and **BBR**$^{8+}$ can be attributed to the greater charge repulsion present in the latter rotaxane, as well as to the comparatively tight fit[68] between the cyclophane components of **BBR**$^{8+}$.

The conversion of **BBR**$^{8+}$ to **BBR**$^{4(+\bullet)}$ was probed (Figure 2a) by UV−vis−NIR spectroscopic monitoring of the

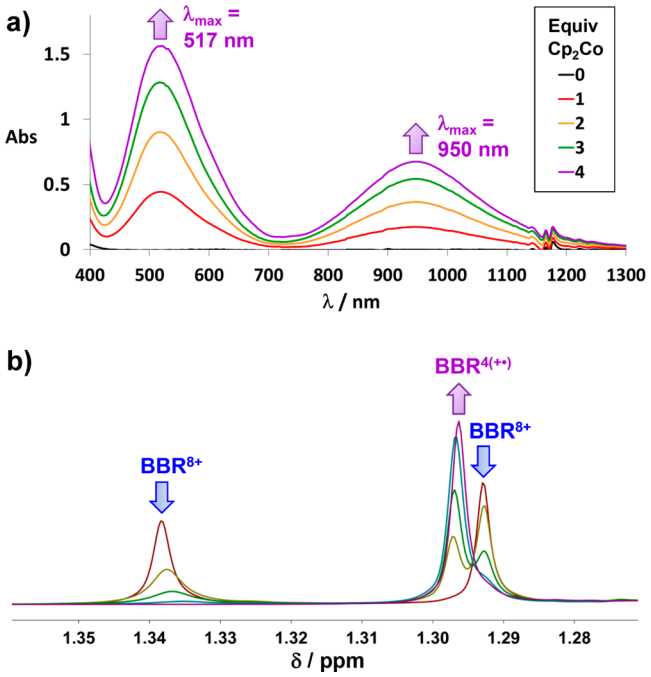

Figure 2. Titrations of solutions of **BBR**·8PF$_6$ with 1 equiv at a time of Cp$_2$Co. (a) UV−vis−NIR spectra of a 0.050 mM solution of **BBR**·8PF$_6$ in MeCN after the addition of 0−4 equiv of Cp$_2$Co. (b) Partial ^{1}H NMR spectra displaying the ^{t}Bu resonances of a 1 mM solution of **BBR**·8PF$_6$ in CD$_3$CN, after the addition of 0−4 equiv of Cp$_2$Co.

sequential addition of 1−4 equiv of the 1 e$^-$ reductant[75] Cp$_2$Co to a solution of **BBR**·8PF$_4$ in MeCN. The resulting spectra exhibit linear increases with each equivalent that is added, indicating that **BBR**$^{8+}$ is converted portionwise directly to **BBR**$^{4(+\bullet)}$. Intermediate oxidation states must, therefore, not be thermodynamically accessible to any significant extent. The spectrum obtained following the addition of 4 equiv of Cp$_2$Co corresponds to full conversion of **BBR**$^{8+}$ to **BBR**$^{4(+\bullet)}$, which exhibits an intense NIR band (λ_{max} = 950 nm) that is very similar to that[16] (λ_{max} = 941 nm) observed for the host−guest complex [**MS⊂*m*-CBPQT**]$^{4(+\bullet)}$. This comparison indicates that this radical ring-in-ring complex provides an accurate coconformational model for the associated cyclophane components of **BBR**$^{4(+\bullet)}$.

^{1}H NMR spectroscopy was also employed to monitor the titration of **BBR**·8PF$_6$ with Cp$_2$Co in CD$_3$CN. The two ^{t}Bu proton resonances of **BBR**$^{8+}$ are observed (Figure 2b) to undergo stepwise decreases in intensities upon sequential addition of Cp$_2$Co, while the single ^{t}Bu resonance of **BBR**$^{4(+\bullet)}$ grows in strength concomitantly. Other ^{1}H resonances of

DOI: 10.1021/acscentsci.7b00535
ACS Cent. Sci. 2018, 4, 362−371

BBR$^{4(+\bullet)}$ are also observed (Figure 3a) in the spectrum after the addition of 4 equiv of the reductant. The signals for both

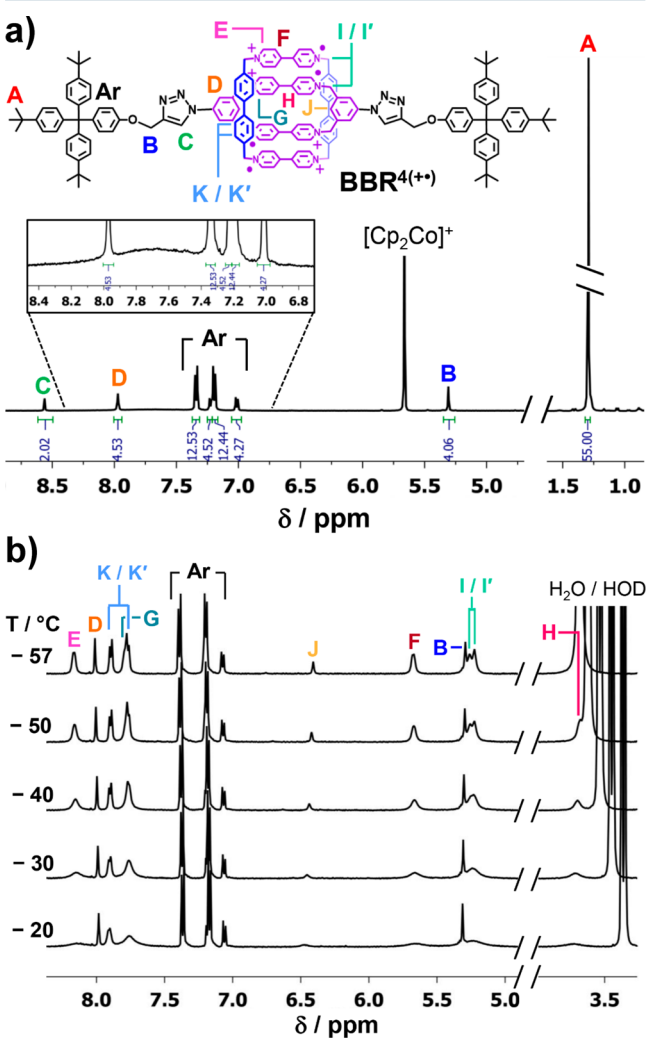

Figure 3. (a) ^{1}H NMR spectrum of a CD_3CN solution of **BBR**$^{4(+\bullet)}$ that was prepared *in situ* by the addition of 4 equiv of Cp_2Co to a solution of **BBR**·8PF_6. The spectrum is abridged in the region of the residual CD_2HCN and HOD signals, and the height of the ^{t}Bu resonance is truncated. See Figure S4 for the full spectrum. (b) Partial ^{1}H NMR spectra, collected over a temperature range of −20 to −57 °C, of a solution of **BBR**$^{4(+\bullet)}$ in CD_3COCD_3 that was prepared *in situ* by stirring a solution of **BBR**·8PF_6 over Zn dust. Although the resonances arising from the **BBR**$^{4(+\bullet)}$ cation are best resolved in the spectrum collected at −57 °C, signal H is obscured by the H_2O/HOD signal at this temperature. In the interest of preserving space, the ^{t}Bu resonance of **BBR**$^{4(+\bullet)}$ is not displayed. See Figure S14 for the full ^{1}H NMR spectrum recorded at −57 °C.

BBR$^{4(+\bullet)}$ and **BBR**$^{8+}$ are observed in the ^{1}H NMR spectra collected during intermediate stages of the titration. See Figures S24–S26. Selective broadening of some resonances of each oxidation state are, however, evident at the midpoint of the titration. Since this broadening does not affect all of the signals, it can be concluded that the two oxidation states do not rapidly undergo degenerate interconversion—a 4-electron based process—on the ^{1}H NMR time scale. Instead, there may be some degree of single-electron transfer to provide **BBR**$^{(7+)(1\bullet)}$ and **BBR**$^{(5+)(3\bullet)}$ transiently, a process which would affect primarily the NMR signals arising from protons that are on or near the cyclophane components.

The ^{1}H NMR spectrum of **BBR**$^{4(+\bullet)}$ exhibits several well-resolved signals, including those for the four outward facing protons of the *m*-phenylene linker, which are located very close to the viologen radical cations. The ability to observe sharp signals from these protons can be attributed to the strong radical-pairing interactions between the two cyclophanes, a phenomenon which provides a diamagnetic ground state. In contrast, the closest observable protons in the ^{1}H NMR spectrum (Figure S6) of the free dicationic diradical dumbbell, ***m*-DBD**$^{2(+\bullet)}$, are the −CH_2O− methylene protons, a full seven bonds away from the *m*-phenylene positions that can be observed in the spectrum of **BBR**$^{4(+\bullet)}$. Other ^{1}H NMR resonances arising from the cyclophane components of **BBR**$^{4(+\bullet)}$ could not be observed individually in the spectra collected at 25 °C, but broad signals, such as that observed in the inset of Figure 3a, can be attributed to these groups. These broad signals are most well-resolved when 3−4 equiv of Cp_2Co has been added, or when Zn dust was used as the reducing agent, but disappear upon the addition of even a small excess (4.25 equiv) of Cp_2Co. See Figures S26 and S27. Further characterization of lower (<4+) oxidation states of this rotaxane is described below in the section "Lower Oxidation States of **BBR**$^{x(+\bullet)}$".

^{1}H NMR spectra of **BBR**$^{4(+\bullet)}$ were collected at reduced temperatures in CD_3COCD_3 in the hopes of resolving the broad resonances observed in the spectra collected at 25 °C. These resonances sharpened and resolved into individual signals in the spectra collected at temperatures between +25 and −57 °C. Resonances for all the possible protons of **BBR**$^{4(+\bullet)}$ can be observed (Figure 3b) clearly at −50 °C. At −57 °C, the proton resonances of the cyclophane units are even better resolved, although one of them becomes obscured by the H_2O/HOD residual signal. The resonances of **BBR**$^{4(+\bullet)}$ integrate appropriately in the spectrum collected at −57 °C, and *J*-coupling (J = 5.4 Hz) can even be discerned for the two viologen Ar−H doublets that do not overlap with other signals. See Figure S15 for a depiction of the integrated spectrum.

The four aromatic resonances of the viologen units can be assigned based on the shielding of the protons that is expected by considering their proximity to other aromatic units. The innermost viologen protons of the smaller cyclophane are, thus, assigned to the most upfield signal since these protons are surrounded on both sides by other viologen units. The 2-positions of the pyridinium groups, in contrast, give rise to ^{1}H NMR signals with normal pyridinum chemical shifts. These protons are not in the proximity of other viologen units because of the nearly perpendicular geometry that is enforced between these units on the smaller cyclophane compared with the larger one. The assumptions of this analysis were validated by ^{1}H NMR spectroscopic studies of the cyclophane[59] ***o*-CBPQT**$^{2(+\bullet)}$, which also exhibits diamagnetic NMR behavior. See Figure S8. The *o*-phenylene linkers of this small cyclophane enforce an eclipsed, rather than perpendicular, alignment of the viologen units, such that the 2- and 3-positions on the pyridinum groups are shielded to a similar extent by the adjacent viologen unit. This geometric arrangement is reflected in the ^{1}H NMR chemical shifts of ***o*-CBPQT**$^{2(+\bullet)}$; the viologen units give rise to more tightly clustered ^{1}H NMR chemical shifts than those observed in the spectra of **BBR**$^{4(+\bullet)}$.

It is remarkable that well-resolved ^{1}H NMR spectra could be obtained for **BBR**$^{4(+\bullet)}$ and ***o*-CBPQT**$^{2(+\bullet)}$. The latter species

DOI: 10.1021/acscentsci.7b00535
ACS Cent. Sci. 2018, 4, 362−371

was first reported[59] ca. 30 years ago, but it was not investigated by ^{1}H NMR spectroscopy even though EPR spectroscopy indicated that it is diamagnetic. To our knowledge,[67,76−80] well-resolved ^{1}H NMR spectra have never been observed for any other diamagnetic viologen radical dimers, which in most cases can be attributed to rapid equilibration between the dimers and a significant concentration of the paramagnetic monomers. It is conceivable that similar processes—equilibration between $\mathbf{BBR}^{4(+\bullet)}$ and a metastable coconformation (MSCC), $\mathbf{BBR}^{4(+\bullet)}_{D}$, in which the two cyclophane components are dissociated from each other—might be responsible for the broadening of the cyclophane resonances in the ^{1}H NMR spectrum of $\mathbf{BBR}^{4(+\bullet)}$ at 25 °C. This possibility can, however, be discounted based on variable scan-rate cyclic voltammetry described in the next section.

Another possible explanation for the selective broadening of the ^{1}H NMR signals of $\mathbf{BBR}^{4(+\bullet)}$ is that rapid electron transfer between $\mathbf{BBR}^{4(+\bullet)}$ and $\mathbf{BBR}^{8+}$ could transiently form $\mathbf{BBR}^{(7+)(1\bullet)}$ and $\mathbf{BBR}^{(5+)(3\bullet)}$, as is invoked (*vide supra*) to account for the broadening of signals of $\mathbf{BBR}^{8+}$ when a large concentration of $\mathbf{BBR}^{4(+\bullet)}$ is present. This explanation is, however, inadequate when it comes to explaining the NMR spectroscopic data of $\mathbf{BBR}^{4(+\bullet)}$ for two reasons: (1) Reduction of $\mathbf{BBR}^{8+}$ with an excess of Zn dust is expected to provide nearly complete and selective conversion to $\mathbf{BBR}^{4(+\bullet)}$ (see Figure S35 for the relevant EPR spectrum), and (2) ***o*-CBPQT$^{2(+\bullet)}$** consistently exhibits sharp ^{1}H NMR resonances at a much higher temperature (+25 °C) than does $\mathbf{BBR}^{4(+\bullet)}$ (−57 °C). This latter observation is particularly significant because the rigid covalent linkers in ***o*-CBPQT$^{2(+\bullet)}$** must greatly reduce the rearrangement energy needed for electron transfer between ***o*-CBPQT$^{2(+\bullet)}$** and its higher oxidation states, such that the ^{1}H NMR spectrum of ***o*-CBPQT$^{2(+\bullet)}$** should be more sensitive to electron transfer processes. Consistent with this assessment, ^{1}H NMR signals could not be observed for a 1:1 ratio mixture of ***o*-CBPQT$^{2(+\bullet)}$** and ***o*-CBPQT^{4+}** in CD_3CN. See Figure S31.

The best explanation for the broadened ^{1}H NMR signals in the case of $\mathbf{BBR}^{4(+\bullet)}$ is that there is a thermally accessible triplet electronic state. Previous DFT calculations[68] on **[MS⊂*m*-CBPQT]$^{4(+\bullet)}$** revealed that its HOMO consists of a bonding combination of the viologen SOMO orbitals, while the LUMO corresponds to an antibonding combination. The lowest energy triplet state of $\mathbf{BBR}^{4(+\bullet)}$ would involve the thermal excitation of an electron across this HOMO−LUMO gap, thus disrupting one of the radical-pairing interactions. The ***o*-CBPQT$^{2(+\bullet)}$** cyclophane presumably has a larger HOMO−LUMO separation because the eclipsed arrangement of its viologen units provides greater orbital overlap.[62] The relative HOMO−LUMO gaps for ***o*-CBPQT$^{2(+\bullet)}$** and $\mathbf{BBR}^{4(+\bullet)}$ were assessed by comparing their NIR absorption bands, which arise[60,61] from the photoinduced promotion of an electron from the HOMO to the LUMO level within radical-paired dimers. It should be noted that the energies of these photoexcitations do not provide a direct measure of the energies of thermally promoted singlet/triplet interconversion because the optical absorption is a singlet-to-singlet transition and is subject to the Franck−Condon principle. Since, however, these effects apply to both ***o*-CBPQT$^{2(+\bullet)}$** and $\mathbf{BBR}^{4(+\bullet)}$, it can be concluded that the HOMO−LUMO gap is larger in this smaller cyclophane (λ_{max} = 850 nm)[59] relative to the rotaxane (λ_{max} = 950 nm, Figure 2a), as expected based on the ^{1}H NMR spectra for each compound. Despite its influence on the ^{1}H NMR spectrum of $\mathbf{BBR}^{4(+\bullet)}$, the triplet state of this rotaxane could not be observed by EPR spectroscopy (see Figure S35) even for samples that were warmed to 90 °C.

Electrochemical Characterization of BBR·8PF$_6$. Cyclic voltammetry was used to probe the interconversion between $\mathbf{BBR}^{8+}$, $\mathbf{BBR}^{4(+\bullet)}$, and a neutral form of this rotaxane $\mathbf{BBR}^{0}$. These are the three oxidation states of the rotaxane that appear to be accessible based on the CV data presented in Figure 4a.

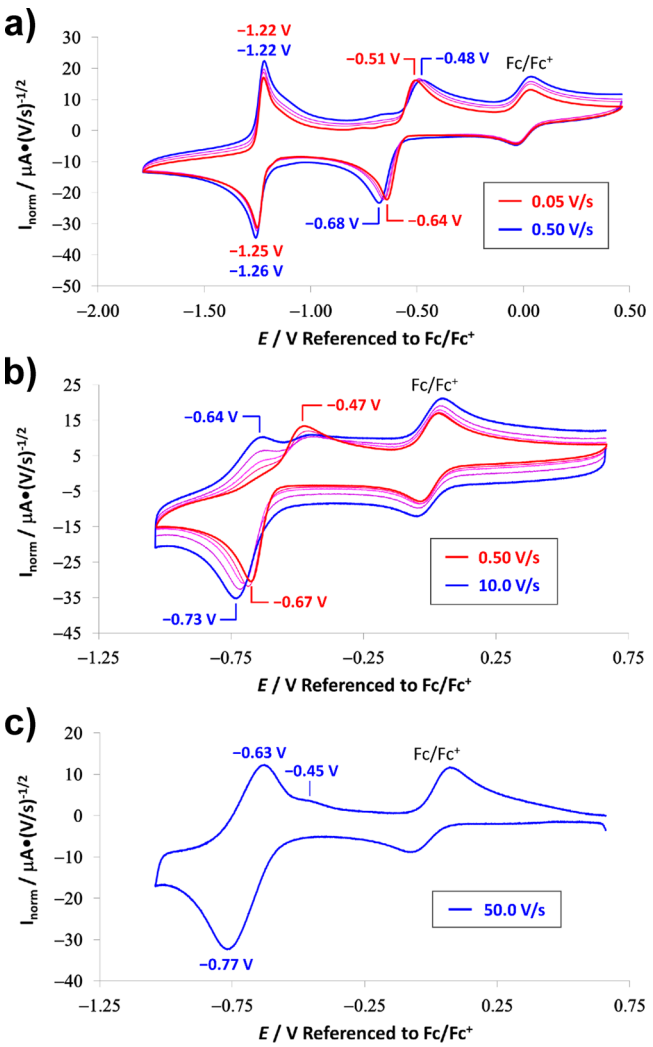

Figure 4. Cyclic voltammograms (CVs) of a 0.125 mM solution of **BBR**·8PF$_6$ in MeCN containing a 0.1 M concentration of [Bu$_4$N][PF$_6$] electrolyte and ferrocene as an internal redox standard. In all the CVs, the current is normalized relative to the square root of the scan rate. (a) Scan rates of 0.05, 0.1, 0.2, and 0.5 V/s with a potential window that includes all accessible oxidation states of the rotaxane. (b) Scan rates of 0.5, 1, 2.5, 5.0, and 10.0 V/s over a potential window that includes only the $\mathbf{BBR}^{8+}$ and $\mathbf{BBR}^{4(+\bullet)}$ oxidation states of the rotaxane. (c) Scan rate of 50.0 V/s over a potential window that includes only the $\mathbf{BBR}^{8+}$ and $\mathbf{BBR}^{4(+\bullet)}$ oxidation states of the rotaxane. The capacitive current at 50.0 V/s was measured independently and subtracted from this CV.

The more negative $\mathbf{BBR}^{4(+\bullet)}/\mathbf{BBR}^{0}$ redox couple exhibits completely reversible behavior at scan rates between 50 and 500 mV/s, while, in contrast, the $\mathbf{BBR}^{8+}/\mathbf{BBR}^{4(+\bullet)}$ redox couple displays a large peak separation ($\Delta E_p \geq 130$ mV) even at the lowest scan rates examined, i.e., 50 mV/s in Figure 4a and 10 mV/s in Figure S38. This large peak separation can be explained by a slow rate of dissociation for the two cyclophanes

DOI: 10.1021/acscentsci.7b00535
ACS Cent. Sci. 2018, 4, 362−371

from the radical-paired state of $BBR^{4(+\bullet)}$, resulting in an overpotential for oxidation back to the BBR^{8+} state. Similar electrochemical behavior was observed[68] previously for the corresponding redox couple of a 1:1 molar ratio mixture of **MS**·$4PF_6$ and ***m*-CBPQT**·$4PF_6$, though, in contrast with BBR^{8+}, reversible behavior was observed for the host–guest complex at sufficiently low scan rates (≤25 mV/s). Thus, the two cyclophane components of $BBR^{4(+\bullet)}$ come apart even more slowly than the two cyclophane components of $[MS\subset m\text{-}CBPQT]^{4(+\bullet)}$, a difference that might be attributed to steric factors associated with the dumbbell component of $BBR^{4(+\bullet)}$.

The more positive redox couple of BBR^{8+} was examined in more detail to determine if the slow kinetics of association observed[68] previously between $m\text{-}CBPQT^{2(+\bullet)}$ and $MS^{2(+\bullet)}$ would be preserved within the context of the rotaxane. As the scan rate was increased beyond 500 mV/s, the CVs of **BBR**·$8PF_6$ revealed the appearance of a new reoxidation wave at potentials that were negative relative to those of the wave that is assigned to the radical-paired state of this rotaxane. See Figure 4b. The appearance of this wave can be attributed to the oxidation of a metastable coconformation (MSCC) $BBR^{4(+\bullet)}{}_D$ in which the two rings are dissociated from each other. Such a wave would appear at higher scan rates if, after reduction of BBR^{8+} to $BBR^{4(+\bullet)}{}_D$, the two cyclophane components came together too slowly to form the associated $BBR^{4(+\bullet)}{}_A$ ground state coconformation (GSCC). The wave corresponding to the $BBR^{4(+\bullet)}{}_A$ state disappears almost completely at a scan rate of 50 V/s, such that the more negative $BBR^{4(+\bullet)}{}_D$ wave is part of a nearly reversible redox couple. The $E_{1/2}$ value (−0.70 V) is similar to those observed[68] for the individual $MS^{4+}/MS^{2(+\bullet)}$ and $m\text{-}CBPQT^{4+}/m\text{-}CBPQT^{2(+\bullet)}$ redox processes and is consistent with the assignment of the wave to a reversible $BBR^{8+}/BBR^{4(+\bullet)}{}_D$ couple.

The electrochemical mechanism in Scheme 4 was used to simulate the CVs of the $BBR^{8+}/BBR^{4(+\bullet)}$ redox couple. It is assumed that, like the individual cyclophanes, this rotaxane undergoes two-electron redox processes. Furthermore, the rate constant, k_1, for the conversion of $BBR^{(6+)(2\bullet)}{}_D$ to $BBR^{(6+)(2\bullet)}{}_A$ can be assumed to be lower than that (k_2) for the conversion of $BBR^{4(+\bullet)}{}_D$ to $BBR^{4(+\bullet)}{}_A$ simply because the latter association process occurs with less charge repulsion. This consideration implies that the pathway associated with k_2 will be the primary route that leads to the formation of the $BBR^{4(+\bullet)}{}_A$ state. From the CV data, it is also evident that $k_{-1} > k_2$ because the metastable coconformation $BBR^{(6+)(2\bullet)}{}_A$ of the 6+ oxidation state does not have a long enough lifetime to permit observation of a $BBR^{(6+)(2\bullet)}{}_A/BBR^{8+}{}_A$ oxidation wave. When these considerations were taken into account, CVs simulated with a rate constant of k_2 = 10–25 s^{-1} provided good agreement[81] with the experimental data relating to the appearance and disappearance of the $BBR^{4(+\bullet)}{}_D/BBR^{8+}{}_D$ and $BBR^{4(+\bullet)}{}_A/BBR^{(6+)(2\bullet)}{}_A$ oxidation waves. See Figure S41 for simulated CVs obtained with k_2 = 15 s^{-1}. The rate constant, k_{-2}, must be orders of magnitude smaller since the $BBR^{4(+\bullet)}{}_D/BBR^{4(+\bullet)}{}_A$ equilibrium lies far toward the associated state.

CV studies demonstrate that electrochemical hysteresis is observed during the switching between BBR^{8+} and $BBR^{4(+\bullet)}$. Thus, this rotaxane preserves the comparatively slow kinetics of association/dissociation observed for the ring-in-ring complex[68] upon which it is based. In contrast, related hexacationic rotaxanes, e.g., **CBPQT-RV-**$[2]R^{6+}$, exhibit[33] 2–3 reversible redox couples associated with the electrochemical switching between the dissociated 6+ state and the associated trisradical 3+ state, even though the corresponding host–guest complexes can exhibit[63,64] some degree of electrochemical hysteresis involving their association/dissociation at elevated scan rates (1–10 V/s). The slow rate of switching between $BBR^{4(+\bullet)}{}_D$ and $BBR^{4(+\bullet)}{}_A$ is particularly notable, given the distinct electronic nature, i.e., open- versus closed-shell electron configurations, of these two states of this rotaxane. Owing to their odd electron count, the trisradical rotaxanes cannot exhibit this same distinction between their associated and dissociated states since all coconformations of **CBPQT-RV-**$[2]R^{3(+\bullet)}$ are paramagnetic.

Lower Oxidation States of $BBR^{x(+\bullet)}$. CV studies indicate that only three thermodynamically stable oxidation states—namely, BBR^{8+}, $BBR^{4(+\bullet)}$, and BBR^{0}—exist for this ring-in-ring rotaxane. These results are consistent with data from Cp_2Co titration experiments on the conversion of BBR^{8+} to $BBR^{4(+\bullet)}$. In contrast, similar studies on the conversion of $BBR^{4(+\bullet)}$ to BBR^{0} reveal that at least two intermediate oxidation states are accessible. This result was evident from changes in the UV–vis–NIR spectrum (Figure 5a) of a solution of **BBR**·$8PF_6$ in Me_2CO[82] as 4–14 equiv of Cp_2Co were added. Nearly identical results are obtained (Figure S19) when employing MeCN as the solvent.

Upon the addition of 5 and 6 equiv of the reductant, the NIR absorption band of $BBR^{4(+\bullet)}$ decreases in step sizes of >30%, and this decrease is accompanied by a shift in wavelength from $\lambda_{max(4equiv)}$ = 950 nm to $\lambda_{max(6equiv)}$ = 926 nm. Both observations indicate that BBR^{0} is not the only product formed upon partial reduction of $BBR^{4(+\bullet)}$, particularly because BBR^{0} does not absorb in the NIR region. The blue shift of the NIR band implies that there is a significant quantity of an intermediate oxidation state of this rotaxane that also features radical-pairing interactions. This new radical-paired state is assigned (Scheme 5) to $BBR^{2(+\bullet)}{}_A$, which features two of the viologen units in a paired radical state and two in their fully reduced state. Owing to the mixed valency of the viologen units in $BBR^{2(+\bullet)}{}_A$, its electronic absorption spectrum is very similar to that of a 1:1 mixture of $BBR^{4(+\bullet)}$ and BBR^{0}, such that the individual

Scheme 4. Proposed Mechanisms of $BBR^{8+}/BBR^{4(+\bullet)}$ Interconversion

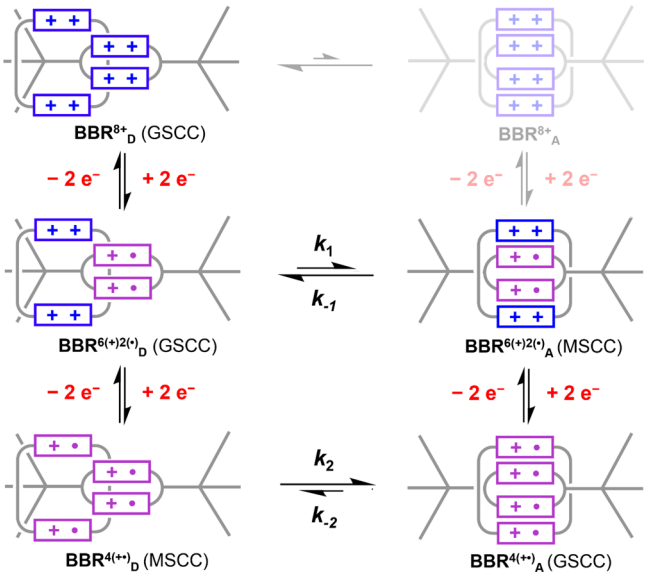

DOI: 10.1021/acscentsci.7b00535
ACS Cent. Sci. 2018, 4, 362–371

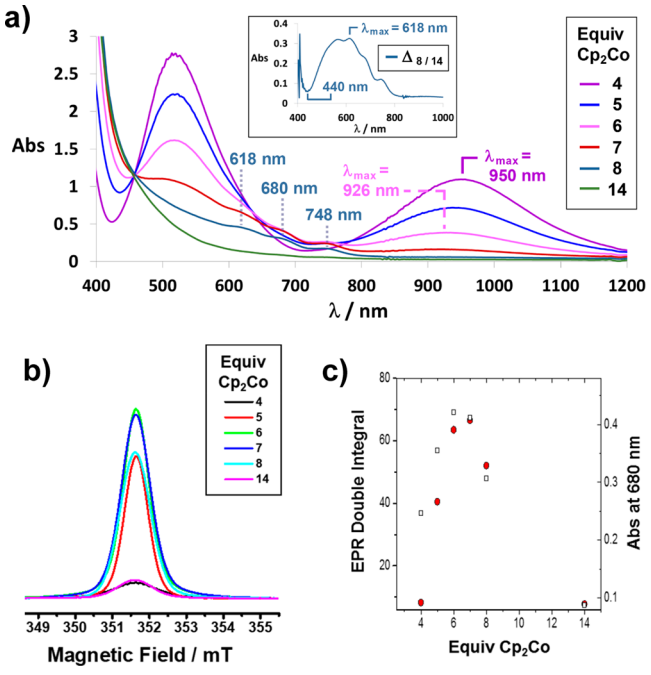

Figure 5. (a) UV−vis−NIR spectra of a 0.33 mM (initial concentration) solution of **BBR**·8PF_6 in Me_2CO following the additions of 4, 5, 6, 7, 8, and 14 equiv of Cp_2Co. The inset depicts the difference between the spectra obtained after adding 8 and 14 equiv of Cp_2Co, with the latter spectrum scaled appropriately to account for different concentrations of the fully reduced viologen units in each sample. (b) Relative integrated EPR signal intensities of 0.25 mM solutions of **BBR**·8PF_6 in Me_2CO after the additions of 4, 5, 6, 7, 8, and 14 equiv of Cp_2Co. See Figure S34 for the full EPR spectra. (c) Comparison of the relative integrated EPR signal intensities (red circles) with the visible light absorption of these samples at 680 nm (squares) that was measured by UV−vis−NIR spectroscopy.

Scheme 5. Electrochemically Hidden Oxidation States of $BBR^{x(+\bullet)}$

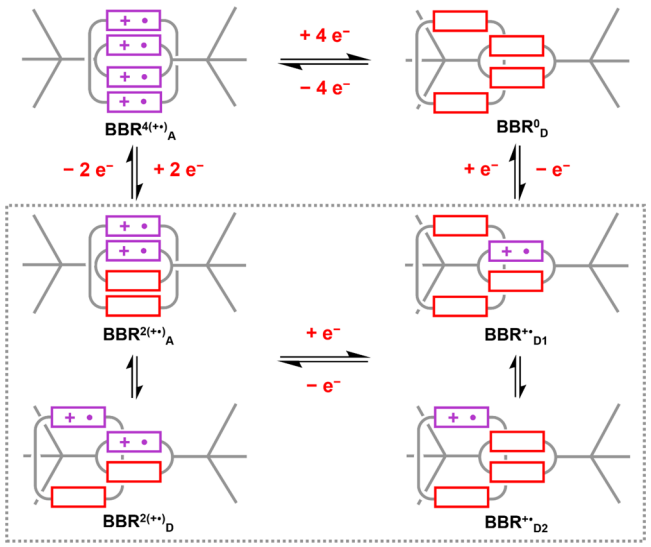

concentrations of these three states of this rotaxane could not be determined in the sample mixture.

In addition to changes in the NIR region, the addition of 6 equiv of Cp_2Co resulted in the observation of subtle features in the visible region of the spectrum that suggested that unpaired viologen radicals are present. These spectroscopic features became more evident after 7 and 8 equiv of Cp_2Co had been added, while the NIR band disappeared almost completely. Note that full reduction of $\mathbf{BBR}^{8+}$ to the neutral $\mathbf{BBR}^{0}$ state is not achieved upon the addition of 8 equiv of Cp_2Co because the Cp_2Co/Cp_2Co^+ redox couple has a potential[75] $E_{Cp2Co/Co+} = -1.3$ V which is not sufficiently negative compared to that of the $\mathbf{BBR}^{4(+\bullet)}/\mathbf{BBR}^{0}$ couple ($E_{BBR4+/BBR0} = -1.24$ V). This limitation was overcome by the addition of a large excess of Cp_2Co (14 equiv) to $\mathbf{BBR}^{8+}$, resulting in complete reduction to $\mathbf{BBR}^{0}$ as indicated by a UV−vis spectrum consistent with the presence of only fully reduced viologen cyclophanes.

The inset in Figure 5a displays a spectrum corresponding only to the radical viologen units of $\mathbf{BBR}^{+\bullet}$. This spectrum was obtained by subtraction of the $\mathbf{BBR}^{0}$ spectrum, with appropriate scaling, from that obtained after the addition of 8 equiv of Cp_2Co to the solution of **BBR**·PF_6. The correct scaling of the $\mathbf{BBR}^{0}$ spectrum was assessed using the assumption that, in the resulting viologen radical spectrum, the absorption maximum at 618 nm and minimum at 440 nm would have a similar ratio of intensities to those observed for other unpaired viologen radicals. From this scaling, it was determined that 85% of the viologen units were in the fully reduced state after the addition of 8 equiv of Cp_2Co, leaving 15% in the radical state. A slightly higher estimate (18%) of the radical concentration was determined by comparing the integrated EPR signal intensity arising from $\mathbf{BBR}^{+\bullet}$ with that of a $\mathbf{MV}^{+\bullet}$ standard. The spectrum of the $\mathbf{BBR}^{+\bullet}$ viologen radical resembles that observed[68] previously for a 1:1 mixture of $\mathbf{MS}^{2(+\bullet)}$ and ***m*-CBPQT**$^{2(+\bullet)}$ under conditions in which there is little association between the two cyclophanes. Thus, it can be concluded that two mixed-valence isomers of $\mathbf{BBR}^{+\bullet}$ are present, which are distinguished by whether the unpaired electron resides on the smaller or larger cyclophane.

The Cp_2Co titration was also monitored by EPR spectroscopy in order to provide the data displayed in Figure 5b,c. The integrated EPR signal intensity increased in approximately equal steps after addition of the fifth and sixth equivalents of the reductant, suggesting that $\mathbf{BBR}^{3(+\bullet)}$ is not a major component of the resulting mixture of $\mathbf{BBR}^{x(+\bullet)}$ oxidation states. The addition of a seventh equivalent of Cp_2Co resulted in a slight increase in the EPR signal intensity, corresponding to the maximum value that was observed during these experiments. This result is consistent with the assignment of the EPR signal primarily to the $\mathbf{BBR}^{+\bullet}$ state of this rotaxane, which is formed upon the addition of 7 electrons to the initial $\mathbf{BBR}^{8+}$ state. The change in the EPR signal intensity between adding the sixth and seventh equivalents was, however, relatively small. This observation indicates that there might be some contribution to the EPR signal from a dissociated $\mathbf{BBR}^{2(+\bullet)}_{D}$ state, as illustrated in Scheme 5, although this possibility can be concluded with less certainty than the existence of the $\mathbf{BBR}^{2(+\bullet)}_{A}$ and $\mathbf{BBR}^{+\bullet}$ states of this rotaxane.

Further information was sought using ^{1}H NMR spectroscopy, but in contrast to the higher oxidation states, only a single set of resonances, corresponding to groups remote from the viologen cyclophanes, could be observed in each of the spectra obtained after adding >4 equiv of Cp_2Co to a solution of $\mathbf{BBR}^{8+}$. See Figures S28−S30. It appears that electrons exchange rapidly between the lower oxidation states of this rotaxane, resulting in the observation of ^{1}H NMR signals that are the average of multiple states, including some with paramagnetic character. Since some of these states involve

DOI: 10.1021/acscentsci.7b00535
ACS Cent. Sci. 2018, 4, 362−371

association between the two rings, while others do not, it can be inferred that the rings associate and dissociate more rapidly in the lower $\mathbf{BBR}^{x(+\bullet)}$ ($x < 4$) oxidation states of this rotaxane than in the higher ones.

CONCLUSIONS

A recently characterized[68] tetracationic tetraradical ring-in-ring complex has now been incorporated into the design of a new rotaxane, $\mathbf{BBR}^{8+}$, which features a cyclophane unit within its dumbbell component. This rotaxane is similar in its design to those of hexacationic rotaxanes based on the tricationic trisradical complex $[\mathbf{CBPQT}\subset\mathbf{MV}]^{3(+\bullet)}$. The properties of $\mathbf{BBR}^{8+}$ are, however, influenced to a great extent by the rigid preorganization of two redox-active viologen units within the cyclophane unit of its dumbbell. The tetracationic charge and physical size of this unit create a significant barrier to the movement of the larger, square-shaped cyclophane from one end of the rotaxane to the other in its $\mathbf{BBR}^{8+}$ oxidation state. Relatively slow kinetics of translational motion are also observed in the case of the reduced $\mathbf{BBR}^{4(+\bullet)}$ state of the rotaxane: strong radical-pairing between the two cyclophanes causes slow dissociation of the rings from this favorable state, while charge repulsion and steric features create a significant barrier to the reverse process. Only in the lower oxidation states of the rotaxane, which feature reduced charge repulsion and weakened radical-pairing, does the larger cyclophane move rapidly along the dumbbell component.

The slow shuttling processes exhibited by $\mathbf{BBR}^{8+}$ and $\mathbf{BBR}^{4(+\bullet)}$ result in easily observable hysteresis for switching between these states, whereas closely related tris-viologen rotaxanes exhibit reversible electrochemical behavior. Furthermore, the associated and dissociated states of $\mathbf{BBR}^{4(+\bullet)}$ have strikingly different electronic properties. The transient $\mathbf{BBR}^{4(+\bullet)}_{\mathbf{D}}$ coconformation exhibits, for example, redox processes comparable to those of individual open-shell viologen cyclophanes, whereas radical-pairing interactions provide diamagnetic character to the $\mathbf{BBR}^{4(+\bullet)}_{\mathbf{A}}$ state while also stabilizing it against oxidation. The distinct electronic features of $\mathbf{BBR}^{4(+\bullet)}_{\mathbf{A}}$ are underscored by the ability to observe well-resolved ^{1}H NMR spectra for this form of the rotaxane.

The striking differences in the electronic properties of the associated and dissociated states of the ring-in-ring rotaxane—as well as marked hysteresis in switching between them—make this rotaxane design promising for the development of molecular electronic materials. More broadly, the ability to identify the reduced $\mathbf{BBR}^{4(+\bullet)}_{\mathbf{A}}$ state of this rotaxane by ^{1}H NMR spectroscopy represents a major step forward in the investigation of complex functional MIMs using radical-pairing interactions. This realization provides a looking glass for peering at the formally radical states of these MIMs, which, in turn, will enable much more detailed understanding of their complex structural features than is available using UV−vis−NIR and EPR spectroscopic methods.

ASSOCIATED CONTENT

Supporting Information

The Supporting Information is available free of charge on the ACS Publications website at DOI: 10.1021/acscentsci.7b00535.

Experimental details, including full synthetic procedures, routine characterization data, cyclic voltammograms, UV−vis−NIR spectra, EPR and ^{1}H NMR spectra, and details of data processing (PDF)

AUTHOR INFORMATION

Corresponding Author

*E-mail: stoddart@northwestern.edu.

ORCID

Mark C. Lipke: 0000-0003-0035-4565
Yilei Wu: 0000-0001-6756-1855
Michael R. Wasielewski: 0000-0003-2920-5440
J. Fraser Stoddart: 0000-0003-3161-3697

Notes

The authors declare no competing financial interest.

ACKNOWLEDGMENTS

This research is part of the Joint Center of Excellence in Integrated Nano-Systems (JCIN) at King Abdulaziz City for Science and Technology (KACST) and Northwestern University (NU). The authors would like to thank both KACST and NU for their continued support of this research. Electron paramagnetic resonance studies were supported by the U.S. National Science Foundation under Grant No. CHE-1565925 (M.R.W.). Y. Wu thanks the Fulbright Scholar Program for a Fellowship and the NU International Institute of Nanotechnology for a Ryan Fellowship.

REFERENCES

(1) Dietrich-Buchecker, C.; Sauvage, J.-P. Interlocking of molecular threads: from the statistical approach to the templated synthesis of catenands. *Chem. Rev.* **1987**, *87*, 795−810.

(2) Amabilino, D. B.; Stoddart, J. F. Interlocked and Intertwined Structures and Superstructures. *Chem. Rev.* **1995**, *95*, 2725−2829.

(3) Sauvage, J.-P., Dietrich-Buchecker, C., Eds. *Molecular Catenanes, Rotaxanes and Knots: A Journey Through the World of Molecular Topology*; Wiley: Weinheim, Germany, 1999.

(4) Stoddart, J. F.; Colquhoun, H. M. Big and Little Meccano. *Tetrahedron* **2008**, *64*, 8231−8263.

(5) Forgan, R. S.; Sauvage, J.-P.; Stoddart, J. F. Chemical topology: complex molecular knots, links, and entanglements. *Chem. Rev.* **2011**, *111*, 5434−5464.

(6) Fahrenbach, A. C.; Bruns, C. J.; Li, H.; Trabolsi, A.; Coskun, A.; Stoddart, J. F. Ground-State Kinetics of Bistable Redox-Active Donor−Acceptor Mechanically Interlocked Molecules. *Acc. Chem. Res.* **2014**, *47*, 482−493.

(7) Bruns, C. J.; Stoddart, J. F. *The Nature of the Mechanical Bond: From Molecules to Machines*; Wiley: Hoboken, NJ, USA, 2017.

(8) Wasserman, E. The Preparation of Interlocking Rings: A Catenane. *J. Am. Chem. Soc.* **1960**, *82*, 4433−4434.

(9) Schill, G.; Lüttringhaus, A. The Preparation of Catena Compounds by Directed Synthesis. *Angew. Chem., Int. Ed. Engl.* **1964**, *3*, 546−547.

(10) Harrison, I. T.; Harrison, S. Synthesis of a stable complex of a macrocycle and a threaded chain. *J. Am. Chem. Soc.* **1967**, *89*, 5723−5724.

(11) Ashton, P. R.; Goodnow, T. T.; Kaifer, A. E.; Reddington, M. V.; Slawin, A. M. Z.; Spencer, N.; Stoddart, J. F.; Vicent, C.; Williams, D. J. A [2]Catenane Made to Order. *Angew. Chem., Int. Ed. Engl.* **1989**, *28*, 1396−1399.

(12) Harrison, I. T. The effect of ring size on threading reactions of macrocycles. *J. Chem. Soc., Chem. Commun.* **1972**, 231−232.

(13) Ashton, P. R.; Bělohradský, M.; Philp, D.; Spencer, N.; Stoddart, J. F. The self assembly of [2]- and [3]-rotaxanes by slippage. *J. Chem. Soc., Chem. Commun.* **1993**, *0*, 1274−1277.

(14) Chiu, C.-W.; Lai, C.-C.; Chiu, S.-H. Threading-Followed-by-Swelling": A New Protocol for Rotaxane Synthesis. *J. Am. Chem. Soc.* **2007**, *129*, 3500−3501.

(15) Barin, G.; Coskun, A.; Friedman, D. C.; Olson, M. A.; Colvin, M. T.; Carmielli, R.; Dey, S. K.; Bozdemir, O. A.; Wasielewski, M. R.;

DOI: 10.1021/acscentsci.7b00535
ACS Cent. Sci. 2018, 4, 362−371

Stoddart, J. F. A Multistate Switchable [3]Rotacatenane. *Chem. - Eur. J.* **2011**, *17*, 213−222.
(16) Vajpayee, V.; Song, Y. H.; Cook, T. R.; Kim, H.; Lee, Y.; Stang, P. J.; Chi, K.-W. A unique non-catenane interlocked self-assembled supramolecular architecture and its photophysical properties. *J. Am. Chem. Soc.* **2011**, *133*, 19646−19649.
(17) Hayashi, R.; Wakatsuki, K.; Yamasaki, R.; Mutoh, Y.; Kasama, T.; Saito, S. Synthesis of rotacatenanes by the combination of Cu-mediated threading reaction and the template method: the dual role of one ligand. *Chem. Commun.* **2014**, *50*, 204−206.
(18) Leigh, D. A.; Marcos, V.; Wilson, M. R. Rotaxane Catalysts. *ACS Catal.* **2014**, *4*, 4490−4497.
(19) Beswick, J.; Blanco, V.; Bo, G. D.; Leigh, D. A.; Lewandowska, U.; Lewandowska, B.; Mishiro, K. Selecting reactions and reactants using a switchable rotaxane organocatalyst with two different active sites. *Chem. Sci.* **2015**, *6*, 140−143.
(20) Galli, M.; Lewis, J. E. M.; Goldup, S. M. A Stimuli-Responsive Rotaxane−Gold Catalyst: Regulation of Activity and Diastereoselectivity. *Angew. Chem., Int. Ed.* **2015**, *54*, 13545−13549.
(21) Lee, A.-L. Supramolecular catalysis: A rotaxane with the golden touch. *Nat. Chem.* **2016**, *8*, 8−9.
(22) Movsisyan, L. D.; Franz, M.; Hampel, F.; Thompson, A. L.; Tykwinski, R. R.; Anderson, H. L. Polyyne Rotaxanes: Stabilization by Encapsulation. *J. Am. Chem. Soc.* **2016**, *138*, 1366−1376.
(23) Ito, K. Novel Cross-Linking Concept of Polymer Network: Synthesis, Structure, and Properties of Slide-Ring Gels with Freely Movable Junctions. *Polym. J.* **2007**, *39*, 489−499.
(24) Sawada, J.; Aoki, D.; Uchida, S.; Otsuka, H.; Takata, T. Synthesis of Vinylic Macromolecular Rotaxane Cross-Linkers Endowing Network Polymers with Toughness. *ACS Macro Lett.* **2015**, *4*, 598−601.
(25) Murakami, T.; Schmidt, B. V. K. J.; Brown, H. R.; Hawker, C. J. One-Pot "Click" Fabrication of Slide-Ring Gels. *Macromolecules* **2015**, *48*, 7774−7781.
(26) Nakahata, M.; Mori, S.; Takashima, Y.; Yamaguchi, H.; Harada, A. Self-Healing Materials Formed by Cross-Linked Polyrotaxanes with Reversible Bonds. *Chem.* **2016**, *1*, 766−775.
(27) Aoki, D.; Aibara, G.; Uchida, S.; Takata, T. A Rational Entry to Cyclic Polymers via Selective Cyclization by Self-Assembly and Topology Transformation of Linear Polymers. *J. Am. Chem. Soc.* **2017**, *139*, 6791−6794.
(28) Collier, C. P.; Mattersteig, G.; Wong, E. W.; Luo, Y.; Beverly, K.; Sampaio, J.; Raymo, F. M.; Stoddart, J. F.; Heath, J. R. A [2]Catenane-Based Solid State Electronically Reconfigurable Switch. *Science* **2000**, *289*, 1172−1175.
(29) Steuerman, D. W.; Tseng, H.-R.; Peters, A. J.; Flood, A. H.; Jeppesen, J. O.; Nielsen, K. A.; Stoddart, J. F.; Heath, J. R. Molecular-Mechanical Switch-Based Solid-State Electrochromic Devices. *Angew. Chem., Int. Ed.* **2004**, *43*, 6486−6491.
(30) Green, J. E.; Choi, J. W.; Boukai, A.; Bunimovich, Y.; Johnston-Halperin, E.; DeIonno, E.; Luo, Y.; Sheriff, B. A.; Xu, K.; Shin, Y. S.; Tseng, H.-R.; Stoddart, J. F.; Heath, J. R. A 160-kilobit molecular electronic memory patterned at 1011 bits per square centimeter. *Nature* **2007**, *445*, 414−417.
(31) Cao, D.; Amelia, M.; Klivansky, L. M.; Koshkakaryan, G.; Khan, S. I.; Semeraro, M.; Silvi, S.; Venturi, M.; Credi, A.; Liu, Y. Probing Donor−Acceptor Interactions and Co-Conformational Changes in Redox Active Desymmetrized [2]Catenanes. *J. Am. Chem. Soc.* **2010**, *132*, 1110−1122.
(32) Fahrenbach, A. C.; Zhu, Z.; Cao, D.; Liu, W.-G.; Li, H.; Dey, S. K.; Basu, S.; Trabolsi, A.; Botros, Y. Y.; Goddard, W. A., III; Stoddart, J. F. Radically Enhanced Molecular Switches. *J. Am. Chem. Soc.* **2012**, *134*, 16275−16288.
(33) Li, H.; Zhu, Z.; Fahrenbach, A. C.; Savoie, B. M.; Ke, C.; Barnes, J. C.; Lei, J.; Zhao, Y.-L.; Lilley, L. M.; Marks, T. J.; Ratner, M. A.; Stoddart, J. F. Mechanical Bond-Induced Radical Stabilization. *J. Am. Chem. Soc.* **2013**, *135*, 456−467.
(34) Barnes, J. C.; et al. A Radically Configurable Six-State Compound. *Science* **2013**, *339*, 429−433.
(35) Götz, G.; Zhu, X.; Mishra, A.; Segura, J.-L.; Mena-Osteritz, E.; Bäuerle, P. π-Conjugated [2]Catenanes Based on Oligothiophenes and Phenanthrolines: Efficient Synthesis and Electronic Properties. *Chem. - Eur. J.* **2015**, *21*, 7193−7210.
(36) Sun, J.; Wu, Y.; Wang, Y.; Liu, Z.; Cheng, C.; Hartlieb, K. J.; Wasielewski, M. R.; Stoddart, J. F. An Electrochromic Tristable Molecular Switch. *J. Am. Chem. Soc.* **2015**, *137*, 13484−13487.
(37) Bissell, R. A.; Cordova, E.; Kaifer, A. E.; Stoddart, J. F. A chemically and electrochemically switchable molecular shuttle. *Nature* **1994**, *369*, 133−137.
(38) Linke, M.; Chambron, J.-C.; Heitz, V.; Sauvage, J.-P.; Semetey, V. Complete rearrangement of a multi-porphyrinic rotaxane by metallation−demetallation of the central coordination site. *Chem. Commun.* **1998**, 2469−2470.
(39) Armaroli, N.; Balzani, V.; Collin, J.-P.; Gaviña, P.; Sauvage, J.-P.; Ventura, B. Rotaxanes Incorporating Two Different Coordinating Units in Their Thread: Synthesis and Electrochemically and Photochemically Induced Molecular Motions. *J. Am. Chem. Soc.* **1999**, *121*, 4397−4408.
(40) Kihara, N.; Hashimoto, M.; Takata, T. Redox Behavior of Ferrocene-Containing Rotaxane: Transposition of the Rotaxane Wheel by Redox Reaction of a Ferrocene Moiety Tethered at the End of the Axle. *Org. Lett.* **2004**, *6*, 1693−1696.
(41) Murakami, H.; Kawabuchi, A.; Matsumoto, R.; Ido, T.; Nakashima, N. A Multi-Mode-Driven Molecular Shuttle: Photochemically and Thermally Reactive Azobenzene Rotaxanes. *J. Am. Chem. Soc.* **2005**, *127*, 15891−15899.
(42) Davidson, G. J. E.; Sharma, S.; Loeb, S. J. A [2]Rotaxane Flip Switch Driven by Coordination Geometry. *Angew. Chem., Int. Ed.* **2010**, *49*, 4938−4942.
(43) Jiménez, M. C.; Dietrich-Buchecker, C.; Sauvage, J.-P. Towards Synthetic Molecular Muscles: Contraction and Stretching of a Linear Rotaxane Dimer. *Angew. Chem., Int. Ed.* **2000**, *39*, 3284−3287.
(44) Tsukagoshi, S.; Miyawaki, A.; Takashima, Y.; Yamaguchi, H.; Harada, A. Contraction of Supramolecular Double-Threaded Dimer Formed by α-Cyclodextrin with a Long Alkyl Chain. *Org. Lett.* **2007**, *9*, 1053−1055.
(45) Romuald, C.; Busseron, E.; Coutrot, F. Very Contracted to Extended co-Conformations with or without Oscillations in Two- and Three-Station [c2]Daisy Chains. *J. Org. Chem.* **2010**, *75*, 6516−6531.
(46) Bruns, C. J.; Li, J.; Frasconi, M.; Schneebeli, S. T.; Iehl, J.; Jacquot de Rouville, H.-P.; Stupp, S. I.; Voth, G. A.; Stoddart, J. F. An Electrochemically and Thermally Switchable Donor−Acceptor [c2]Daisy Chain Rotaxane. *Angew. Chem., Int. Ed.* **2014**, *53*, 1953−1958.
(47) Bruns, C. J.; Frasconi, M.; Iehl, J.; Hartlieb, K. J.; Schneebeli, S. T.; Cheng, C.; Stupp, S. I.; Stoddart, J. F. Redox Switchable Daisy Chain Rotaxanes Driven by Radical−Radical Interactions. *J. Am. Chem. Soc.* **2014**, *136*, 4714−4723.
(48) Wang, Y.; Frasconi, M.; Liu, W.-G.; Sun, J.; Wu, Y.; Nassar, M. S.; Botros, Y. Y.; Goddard, W. A., III; Wasielewski, M. R.; Stoddart, J. F. Oligorotaxane Radicals under Orders. *ACS Cent. Sci.* **2016**, *2*, 89−98.
(49) Leigh, D. A.; Wong, J. K. Y.; Dehez, F.; Zerbetto, F. Unidirectional rotation in a mechanically interlocked molecular rotor. *Nature* **2003**, *424*, 174−179.
(50) Wilson, M. R.; Solá, J.; Carlone, A.; Goldup, S. M.; Lebrasseur, N.; Leigh, D. A. An autonomous chemically fuelled small-molecule motor. *Nature* **2016**, *534*, 235−240.
(51) Kassem, S.; van Leeuwen, T.; Lubbe, A. S.; Wilson, M. R.; Feringa, B. L.; Leigh, D. A. Artificial molecular motors. *Chem. Soc. Rev.* **2017**, *46*, 2592−2621.
(52) Spruell, J. M.; et al. Highly stable tetrathiafulvalene radical dimers in [3]catenanes. *Nat. Chem.* **2010**, *2*, 870−879.
(53) Coskun, A.; Spruell, J. M.; Barin, G.; Fahrenbach, A. C.; Forgan, R. S.; Colvin, M. T.; Carmieli, R.; Benítez, D.; Tkatchouk, E.; Friedman, D. C.; Sarjeant, A. A.; Wasielewski, M. R.; Goddard, W. A., III; Stoddart, J. F. Mechanically Stabilized Tetrathiafulvalene Radical Dimers. *J. Am. Chem. Soc.* **2011**, *133*, 4538−4547.

DOI: 10.1021/acscentsci.7b00535
ACS Cent. Sci. 2018, 4, 362−371

(54) Stoddart, J. F. Putting Mechanically Interlocked Molecules (MIMs) to Work in Tomorrow's World. *Angew. Chem., Int. Ed.* **2014**, *53*, 11102−11104.
(55) Li, H.; Fahrenbach, A. C.; Dey, S. K.; Basu, S.; Trabolsi, A.; Zhu, Z.; Botros, Y. Y.; Stoddart, J. F. Mechanical Bond Formation by Radical Templation. *Angew. Chem., Int. Ed.* **2010**, *49*, 8260−8265.
(56) Gibbs-Hall, I. C.; Vermeulen, N. A.; Dale, E. J.; Henkelis, J. J.; Blackburn, A. K.; Barnes, J. C.; Stoddart, J. F. Catenation through a Combination of Radical Templation and Ring-Closing Metathesis. *J. Am. Chem. Soc.* **2015**, *137*, 15640−15643.
(57) Wang, Y.; Sun, J.; Liu, Z.; Nassar, M. S.; Botros, Y. Y.; Stoddart, J. F. Symbiotic Control in Mechanical Bond Formation. *Angew. Chem., Int. Ed.* **2016**, *55*, 12387−12392.
(58) Kosower, E. M.; Cotter, J. L. Stable Free Radicals. II. The Reduction of 1-Methyl-4-cyanopyridinium Ion to Methylviologen Cation Radical. *J. Am. Chem. Soc.* **1964**, *86*, 5524−5527.
(59) Geuder, W.; Hunig, S.; Suchy, A. Single and double bridged viologenes and intramolecular pimerization of their cation radicals. *Tetrahedron* **1986**, *42*, 1665−1677.
(60) Lü, J.-M.; Rosokha, S. V.; Kochi, J. K. Stable (Long-Bonded) Dimers via the Quantitative Self-Association of Different Cationic, Anionic, and Uncharged π-Radicals: Structures, Energetics, and Optical Transitions. *J. Am. Chem. Soc.* **2003**, *125*, 12161−12171.
(61) Fumanal, M.; Capdevila-Cortada, M.; Ribas-Arino, J.; Novoa, J. J. Electronic Excitation Energies in Dimers between Radical Ions Presenting Long, Multicenter Bonding. *J. Chem. Theory Comput.* **2015**, *11*, 2651−2660.
(62) Geraskina, M. R.; Dutton, A. S.; Juetten, M. J.; Wood, S. A.; Winter, A. H. The Viologen Cation Radical Pimer: A Case of Dispersion-Driven Bonding. *Angew. Chem., Int. Ed.* **2017**, *56*, 9435−9439.
(63) Trabolsi, A.; Khashab, N.; Fahrenbach, A. C.; Friedman, D. C.; Colvin, M. T.; Cotí, K. K.; Benítez, D.; Tkatchouk, E.; Olsen, J.-C.; Belowich, M. E.; Carmielli, R.; Khatib, H. A.; Goddard, W. A., III; Wasielewski, M. R.; Stoddart, J. F. Radically enhanced molecular recognition. *Nat. Chem.* **2010**, *2*, 42−49.
(64) Fahrenbach, A. C.; Barnes, J. C.; Lanfranchi, D. A.; Li, H.; Coskun, A.; Gassensmith, J. J.; Liu, Z.; Benítez, D.; Trabolsi, A.; Goddard, W. A., III; Elhabiri, M.; Stoddart, J. F. Solution-Phase Mechanistic Study and Solid-State Structure of a Tris(bipyridinium radical cation) Inclusion Complex. *J. Am. Chem. Soc.* **2012**, *134*, 3061−3072.
(65) Cheng, C.; McGonigal, P. R.; Liu, W.-G.; Li, H.; Vermeulen, N. A.; Ke, C.; Frasconi, M.; Stern, C. L.; Goddard, W. A., III; Stoddart, J. F. Energetically Demanding Transport in a Supramolecular Assembly. *J. Am. Chem. Soc.* **2014**, *136*, 14702−14705.
(66) Cheng, C.; McGonigal, P. R.; Schneebeli, S. T.; Li, H.; Vermeulen, N. A.; Ke, C.; Stoddart, J. F. An artificial molecular pump. *Nat. Nanotechnol.* **2015**, *10*, 547−553.
(67) To our knowledge, NMR investigations of viologen radical cations have never been reported. We have found that well-resolved ^{1}H NMR signals are not discernible for these organic radicals in solution. Researchers outside of our laboratory have informed us, in private discussions, that they also have been unable to obtain NMR spectra for these compounds, even when radical-pairing ostensibly provides a diamagnetic ground state.
(68) Lipke, M. C.; Cheng, T.; Wu, Y.; Arslan, H.; Xiao, H.; Wasielewski, M. R.; Goddard, W. A., III; Stoddart, J. F. Size-Matched Radical Multivalency. *J. Am. Chem. Soc.* **2017**, *139*, 3986−3998.
(69) Barin, G.; Frasconi, M.; Dyar, S. M.; Iehl, J.; Buyukcakir, O.; Sarjeant, A. A.; Carmieli, R.; Coskun, A.; Wasielewski, M. R.; Stoddart, J. F. Redox-Controlled Selective Docking in a [2]Catenane Host. *J. Am. Chem. Soc.* **2013**, *135*, 2466−2469.
(70) To our knowledge, ref 16 describes the only other example of a rotaxane in which the dumbbell component includes a macrocyclic site on which the outer ring can reside. For the related concept of a catenane that features a macrocyclic component embedded within one of its rings as a recognition unit for the other ring, see ref 71.
(71) Juriček, M.; Barnes, J. C.; Strutt, N. L.; Vermeulen, N. A.; Ghooray, K. C.; Dale, E. J.; McGonigal, P. R.; Blackburn, A. K.; Avestro, A.-J.; Stoddart, J. F. An ExBox [2]catenane. *Chem. Sci.* **2014**, *5*, 2724−2731.
(72) Neelarapu, R.; Holzle, D. L.; Velaparthi, S.; Bai, H.; Brunsteiner, M.; Blond, S. Y.; Petukhov, P. A. Design, Synthesis, Docking, and Biological Evaluation of Novel Diazide-Containing Isoxazole- and Pyrazole-Based Histone Deacetylase Probes. *J. Med. Chem.* **2011**, *54*, 4350−4364.
(73) Dale, E. J.; Vermeulen, N. A.; Juríček, M.; Barnes, J. C.; Young, R. M.; Wasielewski, M. R.; Stoddart, J. F. Supramolecular Explorations: Exhibiting the Extent of Extended Cationic Cyclophanes. *Acc. Chem. Res.* **2016**, *49*, 262−273.
(74) Bryant, R. G. The NMR time scale. *J. Chem. Educ.* **1983**, *60*, 933−935.
(75) Connelly, N. G.; Geiger, W. E. Chemical Redox Agents for Organometallic Chemistry. *Chem. Rev.* **1996**, *96*, 877−910.
(76) Though NMR spectroscopic studies have not, to our knowledge, been reported for viologen radical-cation dimers, solid-state ^{13}C NMR spectra of tetracyanoethylene radical-anion dimers, tetrathiafulvalene radical-cation dimers, and mixed-valency tricyanobenzene trimers have been described. See refs 77 − 80.
(77) Strohmeier, M.; Barich, D. H.; Grant, D. M.; Miller, J. S.; Pugmire, R. J.; Simons, J. Solid-State NMR Spectra and Long Intradimer Bonds in the π-$[TCNE]^{22-}$ Dianion. *J. Phys. Chem. A* **2006**, *110*, 7962−7969.
(78) Bagnato, J. D.; Shum, W. W.; Strohmeier, M.; Grant, D. M.; Arif, A. M.; Miller, J. S. The Structure of Fractionally Charged Tetracyanobenzene^{n-} Present in $[TCNB]^{32-}$. *Angew. Chem., Int. Ed.* **2006**, *45*, 5322−5326.
(79) Miller, J. S.; Novoa, J. J. Four-Center Carbon−Carbon Bonding. *Acc. Chem. Res.* **2007**, *40*, 189−196.
(80) Halling, M. D.; Bell, J. D.; Pugmire, R. J.; Grant, D. M.; Miller, J. S. Solid-State NMR Spectra and Long, Intra-Dimer Bonding in the π-$[TTF]_2^{2+}$ (TTF = Tetrathiafulvalene) Dication. *J. Phys. Chem. A* **2010**, *114*, 6622−6629.
(81) For a given scan rate in the simulated CVs, the ratios of the reoxidation waves for the $\mathbf{BBR}^{4(+\bullet)}_{D}$ and $\mathbf{BBR}^{4(+\bullet)}_{A}$ coconformations are most sensitive to variation of the rate constant k_2, as expected, since this rate constant corresponds to the conversion of $\mathbf{BBR}^{4(+\bullet)}_{D}$ to $\mathbf{BBR}^{4(+\bullet)}_{A}$. There is, however, a smaller dependence of the peak current of the simulated $\mathbf{BBR}^{4(+\bullet)}_{A}$ oxidation wave on the rate constant k_{-1}. As a consequence of these considerations, the simulations allow the value of k_2 to be estimated within a narrow range, but not determined exactly.
(82) Nearly identical results are obtained (Figure S19) when employing MeCN as the solvent. The low solubility of $\mathbf{BBR}^{0}$ in MeCN, however, leads to precipitation of this oxidation state of this rotaxane from solution, making MeCN a less suitable solvent for some measurements. See Figures S20 and S33.

DOI: 10.1021/acscentsci.7b00535
ACS Cent. Sci. 2018, 4, 362−371